J. Fluid Mech. (1969), *vol.* 37, *part* 3, *pp.* 435–448
Printed in Great Britain

The motion of a fluid in a cylindrical container with a free surface following vertical impact

By JEROME H. MILGRAM

Department of Naval Architecture, Massachusetts Institute of Technology, Cambridge, Massachusetts 02139

(Received 1 July 1968 and in revised form 30 October 1968)

The effect of a sudden change in vertical velocity of a vessel partially filled with fluid is considered. It is shown that very small free surface disturbances can be amplified so strongly by a velocity change that instability can occur. This instability frequently causes a jet to emanate from the free surface. Conditions causing free surface disturbances in a vessel in free fall are considered and it is shown that a contact angle between the fluid and the wall of the vessel different from $\frac{1}{2}\pi$ radians can distort the surface in such a way that the amplification and instability upon vertical impact results in a central jet. The results of experiments of this effect are shown. The generation of waves due to transient side wall motions, such as those that might result from fluid pressure at impact, are considered in the appendix. It is shown that such waves would have a different form than those observed in the experiments.

Introduction

When a vessel containing fluid with a free surface undergoes time-varying accelerations, surface waves often occur. The amplification of initial surface disturbances by periodic vertical oscillations of such a vessel has been investigated by Benjamin & Ursell (1954), Dodge, Kana & Abramson (1965) and others. In this paper the effects of transient vertical accelerations and, in particular, the effects of accelerations due to impact, on surface wave generation and amplification are considered.

Controlled experiments were performed and are described in the following sections. However, the initial experiments were performed by dropping various paper cups and tin cans, partially filled with water, on to a floor. Occasionally such an experiment would result in a paper cup splitting its side due to the large impulsive fluid pressure at impact. Since such a transient pressure pulse must cause some wall motion, an analysis of waves generated by axisymmetric wall motion is carried out in the appendix. This analysis predicts maximum initial surface motion near the side walls of the vessel, but experimental results show maximum surface motion near the centre of the surface which occasionally takes the form of a central jet several feet high when the vessel is dropped from only a few inches above the floor. The possibility of large surface motions resulting from sound waves generated at the side or bottom walls has been examined. The result is that the time between impact and arrival of the sound wave at the centre of the surface is an order of magnitude less than the observed time between impact and

jet formation. Therefore, sound waves must be discounted as a possible cause of the observed jets.

Analysis of the amplification of small disturbances present at impact reveals the possibility of large central motions. An extension of the work of Taylor (1953) on the stability of decelerating fluid surfaces in order to take into account the effect of surface tension shows that very small initial disturbances can result in unstable fluid motions for very modest impacts. This results in a central jet, as shown in figure 1, plate 1, which is a sequence of photographs taken 0·033 sec apart following impact of the vessel.

The following three sections are comprised of an analysis of the phenomena related to the generation of large motions of a fluid with a free surface in a rigid vessel following vertical impact. It is shown that surface tension conditions at the side wall can result in distortion of the free surface from that of a plane prior to impact and that the effect of an impact on this distortion can lead to large fluid motions.

The analytical model

Consider a right circular cylindrical vessel of undisturbed radius a, with a solid bottom and filled with fluid to a depth h when the free surface is plane. Axisymmetric motion will be considered with respect to a cylindrical co-ordinate system, fixed to the vessel, with its origin at the centre of the mean free surface and with positive z taken upwards. The fluid is assumed to be inviscid and incompressible with density ρ and to have a surface tension coefficient T on the free surface. The ratio T/ρ will be denoted by τ and the acceleration due to gravity will be denoted by g. The vertical acceleration of the vessel with respect to an inertial frame of reference is called g'.

Small axisymmetric displacements, η, of the free surface are to be considered, for which the surface curvature, κ, is well approximated by the linear relation

$$\kappa = \frac{1}{r}\frac{\partial}{\partial r} r \frac{\partial \eta}{\partial r}. \tag{1}$$

The pressure on the underside of the free surface is then given by

$$P_s = -\frac{T}{r}\frac{\partial}{\partial r} r \frac{\partial \eta}{\partial r} + \text{constant}. \tag{2}$$

The differential equation satisfied by the velocity potential is

$$\nabla^2 \phi = \frac{1}{r}\frac{\partial}{\partial r} r \frac{\partial \phi}{\partial r} + \frac{\partial^2 \phi}{\partial z^2} = 0. \tag{3}$$

The linearized boundary conditions are

$$\phi_z|_{z=-h} = 0, \tag{4}$$

$$\phi_r|_{r=a} = 0 \tag{5}$$

and

$$\phi_{tt} + (g+g')\,\phi_z - \frac{\tau}{r}\frac{\partial}{\partial r} r \frac{\partial \phi_z}{\partial r}\bigg|_{z=0} = 0, \tag{6}$$

which results from combining the kinematic boundary condition

$$\phi_z|_{z=0} = \eta_t \tag{7}$$

and the dynamic boundary condition

$$\phi_t|_{z=0} + (g+g')\,\eta - \frac{\tau}{r}\frac{\partial}{\partial r} r \frac{\partial \eta}{\partial r} = 0. \tag{8}$$

Conditions leading to free surface motion and distortion prior to impact

The equilibrium contact angle of the fluid surface with the side wall of the vessel will be called γ_c so that the angle, γ, of the free surface with a horizontal plane is

$$\gamma = \tfrac{1}{2}\pi - \gamma_c. \tag{9}$$

This leads to the equilibrium boundary condition

$$\left.\frac{\partial \eta}{\partial r}\right|_{r=a} = \tan\gamma. \tag{10}$$

Benjamin & Ursell (1954) have shown that the angle at the side wall between the free surface and the horizontal plane is independent of time so that (10) is true for all time.

The equilibrium free surface shape will first be determined for the case of the vessel at rest. In this case there is no time dependence so (8) becomes

$$g\eta_{\text{rest}} - \frac{\tau}{r}\frac{\partial}{\partial r} r \frac{\partial \eta_{\text{rest}}}{\partial r} = 0, \tag{11}$$

where η_{rest} represents the equilibrium surface elevation when the vessel is at rest. The solution of (11) subject to (10) is

$$\eta_{\text{rest}} = \frac{\tan\gamma}{\sqrt{(g/\tau)}\, I_1(\sqrt{(g/\tau)}\, a)} I_0(\sqrt{(g/\tau)}\, r) + \text{constant}. \tag{12}$$

When the vessel is in free fall, $g' = -g$ so the equilibrium pressure in the fluid must everywhere be the same, and thus the equilibrium free surface shape is that of a spherical cap with the angle between the edge of the free surface and the horizontal plane being γ. For these conditions the equilibrium free surface shape is given by

$$\eta_{\text{free}} = \sqrt{\left(\frac{a}{\tan^2\gamma}(1+\tan^2\gamma) - r^2\right)} + \text{constant}. \tag{13}$$

As an example, graphs of the two equilibrium functions for (12) and (13) are shown in figure 2 for $\gamma = 0{\cdot}5$ radians, $a = 1{\cdot}35$ in., $g = 387$ in./sec^2, and $\tau = 4{\cdot}34$ in.^{3}/sec^2. Typical values for γ are between $-0{\cdot}2$ and $+1{\cdot}5$, depending on the materials comprising the walls of the vessel and the fluid, as well as the wall roughness. Thus the equilibrium free surface shapes can be quite different with and without the effect of gravity present (see figure 2). If the vessel is released from a state of rest to a state of free fall the free surface will oscillate about its new equilibrium shape. Therefore the shape and velocity of the free surface are dependent on the time between release of the vessel and the time of impact.

Since the fluid motion following impact is mainly affected by the shape of the free surface at impact and the speed of the vessel at impact (as is shown subsequently), this motion should be dependent upon the height from which the vessel was dropped.

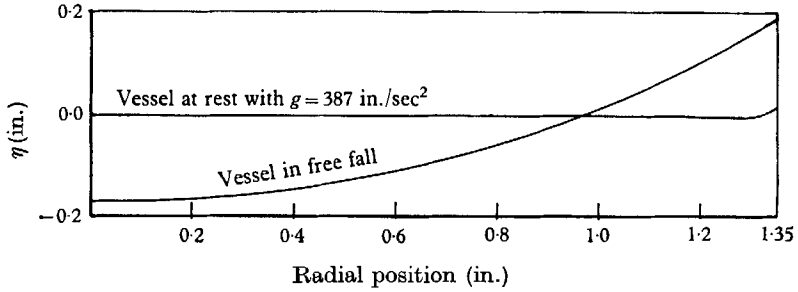

FIGURE 2. Equilibrium free surface shapes for a fluid with a contact angle of $(\pi/2-0{\cdot}5)$ radians on the side wall. The vessel radius is 1·35 in.

The amplification of fluid motion by impact

During free fall $g' = -g$ so there is no body force on the fluid in the reference frame of the vessel. For axisymmetric motion the velocity potential can be expanded as

$$\phi^- = \sum_{n=1}^{\infty} A_n^- J_0(\kappa_n r)\cosh \kappa_n(z+h)\exp\{i\omega_n^- t\}, \tag{14}$$

where

$$J_1(\kappa_n a) = 0 \tag{15}$$

and

$$(\omega_n^-)^2 = \tau\kappa_n^3 \tanh(\kappa_n h). \tag{16}$$

Similarly

$$\eta_t^- = \sum_{n=1}^{\infty} \kappa_n A_n^- J_0(\kappa_n r)\sinh(\kappa_n h)\exp\{i\omega_n^- t\} \tag{17}$$

and

$$\eta^- = \sum_{n=1}^{\infty} \frac{\kappa_n A_n^-}{i\omega_n^-} J_0(\kappa_n r)\sinh(\kappa_n h)\exp\{i\omega_n^- t\}. \tag{18}$$

Following impact, the expressions for ϕ^+, η_t^+, and η^+ are the same as those above, with the A_n^-'s replaced with A_n^+'s and ω_n^- replaced by ω_n^+. If the vessel bounces (16) is valid for ω_n^+ until the vessel again impacts. If the vessel does not bounce,

$$(\omega_n^+)^2 = (g\kappa_n + \tau\kappa_n^3)\tanh \kappa_n h. \tag{19}$$

The dynamic boundary condition on each mode is

$$\phi_t|_{z=0} + (g+g')\eta + \tau\kappa_n^2\eta = 0. \tag{20}$$

There is an impulsive contribution to g' at impact whose time integral U is equal to the change of velocity of the vessel in an inertial reference frame upon impact. Integrating (20) from $t = 0^-$ to $t = 0^+$ gives

$$[\phi^+ - \phi^-]_{z=0} = -U[\eta]_{t=0}. \tag{21}$$

The physical quantities represented by complex equations such as (17) and

(18) will be taken as the real parts of these equations. For continuity in the surface elevation during impact,

$$\frac{\operatorname{Im} A_n^+}{\omega_n^+} = \frac{\operatorname{Im} A_n^-}{\omega_n^-}. \tag{22}$$

Equations (14), (18) and (21) require that

$$\operatorname{Re} A_n^+ = -U\sqrt{\left(\frac{\tanh(\kappa_n h)}{\tau\kappa_n}\right)}\operatorname{Im} A_n^- + \operatorname{Re} A_n^-. \tag{23}$$

Equation (22) shows that at impact the imaginary part of the coefficient of each mode jumps in such a way that the wave amplitude associated with this part of the coefficient is unchanged, but the surface velocity changes such that a change in wave frequency is consistent with fixed amplitude. Equation (23) shows an augmentation to the real part of the coefficient of each mode at impact proportional to the imaginary part of that coefficient just prior to impact with a negative constant of proportionality. Therefore, there is an augmentation to the velocity of each mode at impact, proportional to and of opposite sign than, the displacement in this mode at impact. *A surface depression in the n-th mode at impact results in an augmentation in upward velocity in this mode at impact.*

The stability of large waves

The stability of gravity waves in an accelerating vessel was studied theoretically by Taylor (1950) and experimentally by Lewis (1950) with the conclusion that the waves will be unstable if the downward acceleration of the vessel exceeds g, the acceleration due to gravity. Taylor (1953) concluded that a standing wave form will become unstable if the downward acceleration at any point on the free surface exceeds g.

When the effect of surface tension is considered, it can be shown by methods similar to those used by Taylor that a deep water wave of circular wave-number k will become unstable if the downward acceleration of the free surface exceeds $g + \tau k^2$, measured with respect to an inertial frame of reference. If the fluid is in free fall, the minimum downward free surface acceleration, measured in a reference frame that is in free fall, needed to produce free surface instability is τk^2. These results are based on the linearized relation for the surface curvature (1). If terms of order two in η are taken into account, the curvature is given by

$$\kappa = \frac{1}{r}\frac{\partial}{\partial r} r \frac{\partial \eta}{\partial r}\left[1 - \frac{3}{2}\left(\frac{\partial \eta}{\partial r}\right)^2\right]. \tag{24}$$

The restoring force due to surface tension is less than or equal to that predicted by linear theory. Therefore the stability of the free surface will be equal to or less than that predicted by linear theory.

For many axisymmetric waves the maximum surface deceleration is on the axis so the surface is most unstable there. When an instability occurs there, it results in a central jet. Some jets themselves are unstable with respect to disintegration into drops. The static varicose instability with an axial wavelength

of 4·5 times the jet diameter, described by Rayleigh (1879), appears to be the mechanism of disintegration exhibited in figure 1, plate 1.

If a jet forms, the maximum height any fluid in the jet can attain in an inertial co-ordinate system is the total head this fluid has just when the jet starts. In most cases, the fluid initially having the largest head will not attain this height, since the effect of surface tension will reduce its head during formation of the jet.

Experiments

The cylindrical vessel used for the experiments had an inside radius of 1·35 in., a side wall thickness of 0·1875 in., a bottom thickness of 1 in. and a height of approximately 4 in. The bottom was made of aluminium and the side was made of clear hard polystyrene plastic to allow photographs of the fluid from the side. The vessel was fitted with two steel runners, each running in an axial direction with a length of approximately 4 in. and a width of 0·25 in. These runners slid in bronze tracks which were affixed in a very rigid frame. By accurate grinding of the runners and tracks and proper shimming of the tracks, there was essentially no constraint on vertical motion of the vessel, but transverse motions were limited to approximately 0·001 in. The vessel was filled with fluid to a depth of 2·5 in. and released such that it fell 20 in. before impacting on a 1·5 in. thick aluminium plate which formed the base of the framework of the apparatus. The approximate velocity at impact was 124 in./sec with a free fall time of 0·32 sec. Numerous photographs of the fluid were taken by high-speed photography in Professor H. Edgerton's Stroboscopic Laboratory at M.I.T. The jet height after impact was found to depend on the distance the vessel fell in a non-monotonic fashion. However, for all experiments that were photographed, the vessel fell a distance of 20 in., starting from rest, before impact.

Experiments were carried out with four fluids. They were tap water, deaerated tap water, a solution of a small quantity of liquid soap in deaerated tap water, and glycerin. The fluids have almost identical densities, except for glycerin which has a specific gravity of 1·26. Glycerin was used as one of the fluids because it has a vapour pressure less than 0·01 times that of water and a viscosity of about 1000 times that of water. Thus with glycerin, viscous effects will be much stronger and cavitation effects will be much weaker than with water. The ordinary tap water is much more susceptible to cavitation than the deaerated tap water. The soap solution has a lower surface tension than water and the preceding theory indicates that the surface tension is an important parameter.

The contact angle of the free surface with the wall is dependent on the relative surface tensions of the air-fluid and fluid-wall interfaces. Figure 3, plate 2, shows photographs of the vessel at rest when it contains each of the four fluids. This figure shows significantly positive values of γ for all the fluids except the deaerated tap water where γ is nearly zero. The fact that the ordinary tap water has a larger value of γ than does the deaerated water may be due to contaminants other than air as the two samples of water were taken from the tap and corresponding experiments performed at different times.

Figure 1, plate 1, is a sequence of photographs of the ordinary tap water taken

0·033 sec apart starting must before impact of the vessel. This figure shows that the vessel bounced upon initial impact. These photographs were made by panning the camera with the shutter open while the strobe lamp flashed at a rate of thirty flashes per second. The illumination was reflected from a white surface behind the vessel through the vessel walls and the fluid to the camera. In the first frame following impact, the jet is already over 4 in. in height so the initial stage of the motion is over. In the first few frames, the root of the jet is quite axisymmetric with some circumferential modulation above it. For times greater than 0·1 sec after impact, the upper portion of the jet is relatively axisymmetric and a varicose instability leading to the disintegration of the jet into drops is evident.

Figure 4, plate 3, is a similar sequence of photographs with the same flash rate as before, but with deaerated tap water used for the fluid. Figure 5, plate 3, shows results with the soap solution and figure 6, plate 4, shows the results with glycerin. Figure 7, plate 4, shows a sequence of photographs of the soap solution surface prior to impact. The motion of the fluid during this time is evident.

Figure 8, plate 5, shows photographs of a number of impacts, each one with a different time delay between impact and the time of taking the picture. The maximum time delay is 1 msec. For this figure the illumination was reflected off the vessel and fluid to the camera. The single flash strobe lamp was triggered by a signal at impact coming from a microphone clamped to the frame of the apparatus and then through a time delay circuit. Just following impact, a considerable distortion of the free surface is evident and there is some cavitation. For times greater than 0·2 msec. after impact, the cavitation appears to be restricted to a region near the bottom of the vessel. By 0·5 msec after the impact, the jet has formed. One msec after impact, instability has occurred and the jet is about 1 in. high.

Figure 9, plate 6, shows photographs of the vessel filled with deaerated water taken less than 10^{-5} sec after impact and at 10^{-3} sec after impact. Figure 10, plate 7, shows similar photographs with soap solution in the vessel. These photographs show no evidence of cavitation. For these photographs the method of illumination used in figure 8 was employed. Small scale raggedness of the free surface just following impact can be seen. Such raggedness also exists in the case shown in figure 8, plate 5, but the front lighting used in that figure does not show this effect as clearly as the back lighting used for figure 9, plate 6, and figure 10, plate 7.

Interpretation of experimental results

The time interval between impact and jet formation in the experiments that were photographed was about 5×10^{-4} sec. A radial sound wave originating at the vessel walls at impact would arrive at the centre of the free surface about 2×10^{-5} sec after impact. Therefore the effect of sound waves is not important in the generation of fluid motion leading to the observed central jet formation. However, it is quite likely that the sound waves are important in the generation of the surface raggedness observed about 10^{-5} sec after impact.

The experiments with ordinary tap water exhibit considerable cavitation which would generate waves if it caused radial flow. It has been shown by Knapp (1958) and Johnson (1965) that small air bubbles serve as nuclei for cavitation, and since such bubbles tend to adhere to the sides of the vessel, it is possible that cavitation results in radial flow. However, as shown in the appendix, this would result in more surface motion at the side wall than at the centre of the surface just after impact, whereas the reverse situation was observed.

The cavitation is thought to be caused by the rarefraction sound wave reflected downwards from the free surface when the impact compression wave is incident upon it. The cavitation bubbles soon start to collapse (figure 8). The normal bubble collapse is temporarily hastened by the impact sound wave when it becomes a compression wave again after two more reflexions. The bubble collapse causes a free surface deceleration that could lead to instability. However, this surface deceleration would be either relatively uniform or strongest near the vessel walls which would not lead to a central jet. Because of this, as well as the fact that large jets were observed in the absence of cavitation in deaerated water, soap solution and glycerin, it is clear that cavitation is not important in causing the large surface motion following impact that was observed.

The jet formed following impact of the deaerated tap water was significantly smaller than the jets formed following impact of the ordinary tap water or soap solution. Figure 3, plate 2, shows that the angle between the free surface and the horizontal plane is much smaller with the deaerated tap water than with the other fluids. The preceding theory indicates that for this case a smaller jet is to be expected.

The example of waves due to side wall motion solved in the appendix is not intended to be completely representative of the experiments. However, the general form of the results of this example is intended to be representative of experimental results to within an order of magnitude. In the example, the minimum free surface deceleration needed to cause instability is exceeded, but the maximum dynamic head at the centre of the surface is on the order of 0·1 in. and some experimentally observed jets were two hundred times as high as this. Furthermore, the example indicates maximum vertical velocity and maximum vertical deceleration of the surface at the side wall whereas maximum fluid motion was observed at the centre of the free surface. Therefore, waves due to side wall motion represent only a small influence on the motion observed in the experiments.

Figure 8, plate 5, shows a distortion of the free surface, at a time less than 10^{-5} sec after impact, approximately 0·3 in. deep. The predominent part of the displacement is in the first mode. For the conditions of the experiments with water, the following values hold: $g = 387$ in./sec; $\tau = 4{\cdot}34$ in.^{3}/sec^2; $k = 2{\cdot}84$ in.$^{-1}$; $\omega_1^- = 9{\cdot}93$ radians/sec; $\omega_1^+ = 38{\cdot}2$ radians/sec if the vessel does not bounce, $\omega_1^+ = 9{\cdot}93$ radians/sec if the vessel bounces; $U = 124$ in./sec if the vessel does not bounce, $U > 124$ in./sec if the vessel bounces. The ratios of amplitudes of surface elevation, acceleration, and velocity in the first mode, to initial elevation in the first mode are denoted by R_η, R_a, and R_v respectively. These ratios can be obtained from (18) and (23). Using the values for the parameters of the experiment listed above and assuming there is no fluid velocity with respect to the vessel just

prior to impact gives: $R_\eta = 35{\cdot}2$ if the vessel bounces, $R_\eta = 9{\cdot}15$ if the vessel does not bounce; $R_a = 3{,}480$ sec if the vessel bounces, $R_a = 13{,}400$ sec if the vessel does not bounce; $R_v = 350$ sec.

The critical surface deceleration which must be exceeded to allow instability is 35 in./sec^2 if the vessel bounces and 422 in./sec^2 if the vessel does not bounce. In all experiments, the vessel bounced. Figure 11 shows graphs of theoretical

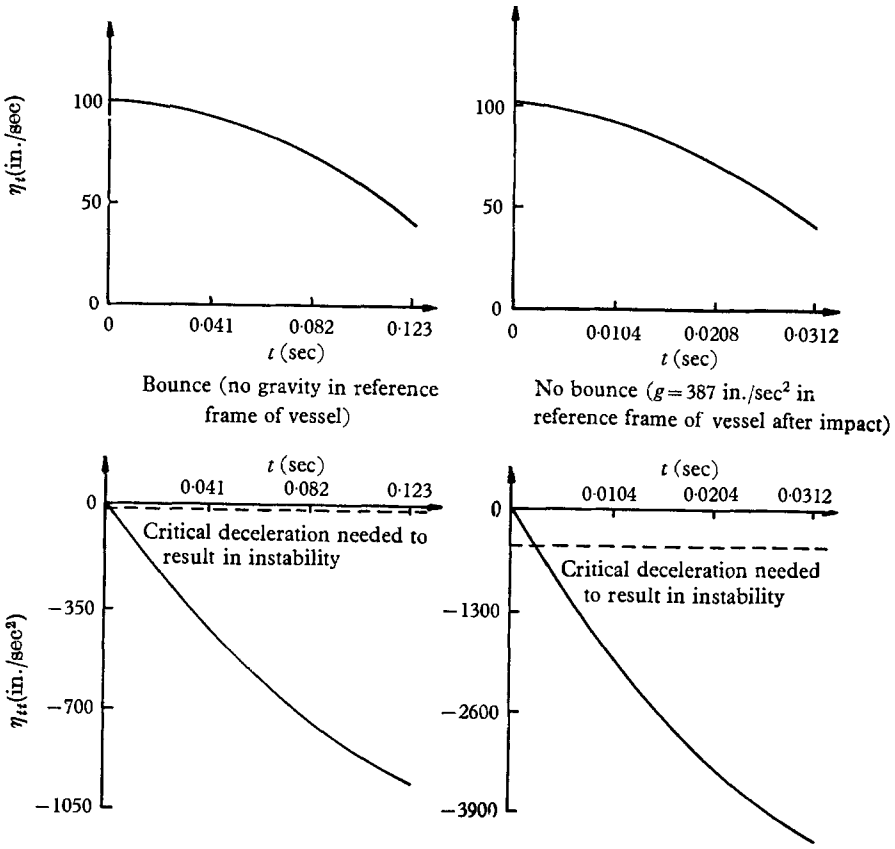

FIGURE 11. Surface velocity and acceleration at the centre of the surface following impact for an initial distortion in the first mode with a central depression of 0·3 in.

values of the free surface velocity and acceleration following impact for the conditions listed above. For this case, with an initial depression at the centre of the surface, the velocity is maximum just after impact and at this time the acceleration is zero and going negative. The critical surface deceleration is reached so soon after impact that the surface velocity has decreased very little from its maximum value at this time. The minimum initial first mode elevation amplitude needed to allow instability is 0·010 in. if the vessel bounces and 0·0315 in. if the vessel does not bounce. A very small initial surface disturbance will result in instability.

When γ is not equal to zero, the shape of the free surface at impact depends on the time interval that the vessel was in free fall. During this time the free

surface oscillates about its equilibrium shape for free fall as can be seen in figure 7, plate 4. This explains why the dependence of jet height on free fall distance is not monotonic.

Conclusions

When a vessel containing fluid with a free surface undergoes impact, there are a number of effects that can lead to free surface motion relative to the vessel. These effects include vessel wall motion due to the fluid pressure at impact, and cavitation due to the rarefraction sound wave reflected downward from the free surface when the impact compression wave is incident upon it. However, the largest surface motion is usually due to Taylor decelerating surface instability caused by the amplification of free surface disturbances by impact. Such a disturbance will occur when the contact angle of the free surface with the wall of the vessel is not 90 degrees, as the equilibrium free surface shapes are then different for the vessel in free fall and for the vessel at rest.

Appendix. Waves due to side wall motion

In this appendix, waves due to axisymmetric side wall motion of the vessel are considered. This motion is taken to be of a form such that the radius of the vessel is given by $a + q(z)f(t)$. This is not the most general form of side wall motion, but serves to bring out the salient effects. This leads to the side wall boundary condition

$$[\phi_r]_{r=a} = q(z)f'(t). \tag{25}$$

The initial conditions are

$$\phi(r, z, 0) = \eta(r, 0) = \eta_t(r, 0) = 0. \tag{26}$$

The problem to be solved in order to determine the velocity potential due to side wall motion is represented by equations (3), (4), (6), (25) and (26). The direct application of Laplace transform methods to initial value problems of this type, which have a continuous spectrum of permissible wave-numbers, gives solutions in terms of infinite series of contour integrals whose evaluations are very tedious. This difficulty is circumvented here by means of a different method of solution. Let

$$\phi(r, z, t) = \phi_1(r, z, t) + \phi_2(r, z, t), \tag{27}$$

where both ϕ_1 and ϕ_2 satisfy

$$\nabla^2\phi_i = 0 \quad (i = 1, 2), \tag{28}$$

and

$$\phi_{i_z}|_{z=-h} = 0 \quad (i = 1, 2). \tag{29}$$

Let ϕ_1 satisfy the inhomogeneous side wall boundary condition

$$\phi_{1_r}|_{r=a} = q(z)f'(t) \tag{30}$$

and the upper boundary condition of a plane free surface

$$\phi_{1_z}|_{z=0} = \text{function of time only.} \tag{31}$$

Equation (27) then determines the following boundary conditions for ϕ_2:

$$[\phi_{2_r}]_{r=a} = 0, \tag{32}$$

$$\left[\phi_{2_{tt}} + g\phi_{2_z} - \frac{\tau}{r}\frac{\partial}{\partial r} r \frac{\partial}{\partial r}\phi_{2_z}\right]_{z=-h} = -\left[\phi_{1_{tt}} + g\phi_{1_z} - \frac{\tau}{r}\frac{\partial}{\partial r}\frac{r\partial}{\partial r}\phi_{1_z}\right]_{z=-h}. \tag{33}$$

The solution to (28)–(31) for ϕ_1 is

$$\phi_1 = -f'(t)\left\{\frac{A_0}{a}\left(z^2 + 2zh - \frac{r^2}{2}\right) + \sum_{n=1}^{\infty} A_n h \cos\frac{n\pi z}{h} I_0\left(\frac{n\pi r}{h}\right)\right\}, \tag{34}$$

where

$$A_0 = \frac{1}{h}\int_{-h}^{0} q(z)\,dz \tag{35}$$

and

$$A_n \frac{\int_{-h}^{0} q(z)\cos(n\pi z/h)\,dz}{h n\pi I_1(n\pi a/h)}. \tag{36}$$

The free surface elevation, η_1, associated with ϕ_1 is then

$$\eta_1 = -2h/a\, A_0 f(t). \tag{37}$$

ϕ_2 will be expressed in terms of its Laplace transform ψ_2 by

$$\phi_2(r,z,t) = \frac{1}{2\pi i}\int_{\sigma-i\infty}^{\sigma+i\infty} \psi_2(r,z,s)\, e^{st}\,ds, \tag{38}$$

where

$$s = \sigma + i\omega \tag{39}$$

The solution to the problem posed by the Laplace transforms of (28), (29), (32) and (33) is then

$$\psi_2(r,z,s) = \sum_{n=1}^{\infty} Q_n(s) J_0(k_n r)\cosh k_n(z+h), \tag{40}$$

where

$$J_1(k_n a) = 0 \tag{41}$$

and

$$Q_n(s) = \frac{-2s^3F(s)\left[\dfrac{A_0}{k_n^2} - \displaystyle\sum_{m=1}^{\infty} \frac{m\pi A_m}{(m^2\pi^2/h^2) + k_n^2} I_1\left(\frac{m\pi a}{h}\right)\right]}{a\cosh(k_n h) J_0(k_n a)[s^2 + p_n^2]}. \tag{42}$$

where

$$p_n^2 = (gk_n + \tau k_n^3)\tanh(k_n h). \tag{43}$$

The free surface elevation, η_2, associated with ϕ_2 is found by substitution of (38), (40) and (42) into (8). This gives

$$\eta_2(r,t) = \frac{1}{2\pi i}\int_{\sigma-i\infty}^{\sigma+i\infty} \sum_{n=1}^{\infty} -2s^2F(s)\frac{\dfrac{A_0}{k_n} - \displaystyle\sum_{m=1}^{\infty}\frac{m\pi A_m k_n}{m^2\pi^2/h^2 + k_n^2} I_1\left(\frac{m\pi a}{h}\right)}{a J_0(k_n a)[s^2 + p_n^2]} \times J_0(k_n r)\tanh(k_n h)\, e^{st}\,ds. \tag{44}$$

It should be noted that the only singularities in the integrand of (44), except for the one at infinity due to e^{st}, are at $s = 0$, $\pm ip_n$ and at the poles of $F(s)$. Therefore, η_2 will be equal to the sum of the residues at these poles since the integral over the large semicircle encompassing the left half-plane is zero due to the term e^{st}.

Note that in this case the k_n's are fixed so when the inverse Laplace transformation is performed by integrating over s, the only s dependence of the inte-

grand is in explicit form. It is important to note that the terms in the summation over n in (44) all have the same sign at the wall, but have alternating signs at the centre of the free surface. In the next section an example is done.

Example

For this example, suppose

$$A_n = 0, \quad n \neq 0. \tag{45}$$

This means that the radius of the vessel undergoes uniform motion, independent of z.

Let
$$f(t) = \begin{cases} \frac{1}{2}(1-\cos 2\pi t/\xi), & 0 \leqslant t \leqslant \xi, \\ 0 \quad , & \text{otherwise} \end{cases} \tag{46}$$

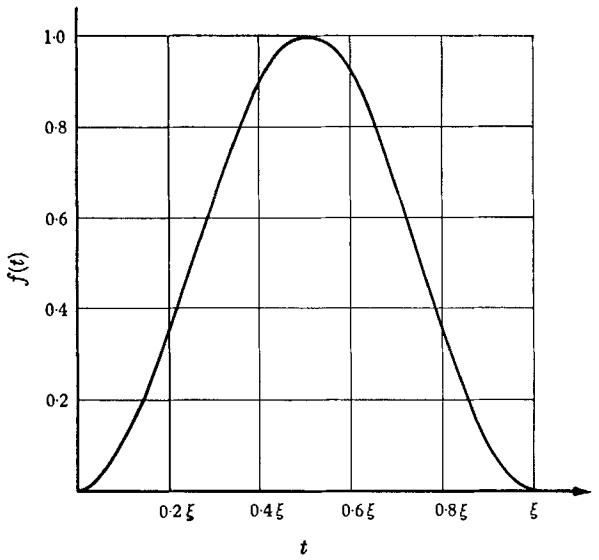

FIGURE 12. The pulse $f(t)$ used for example of waves due to side wall motion.

This pulse is shown in figure 12. For this pulse

$$F(s) = \tfrac{1}{2}(1-e^{-s\xi})\frac{\omega_0^2}{s(s^2+\omega_0^2)}, \tag{47}$$

where
$$\omega_0 = 2\pi/\xi. \tag{48}$$

Using this expression for $F(s)$ in (43) gives

$$\eta_2 = \frac{A_0}{a}\sum_{n=1}^{\infty}\frac{\omega_0^2\tanh(k_n h)J_0(k_n r)}{k_n(p_n^2-\omega_0^2)J_0(k_n a)}\begin{cases} 0 \quad , & t \leqslant 0, \\ \cos p_n t - \cos\omega_0 t \quad , & 0 < t \leqslant \xi, \\ \cos p_n t - \cos p_n(t-\xi), & t > \xi. \end{cases} \tag{49}$$

Also,
$$\eta_1 = \frac{h}{a}A_0\begin{cases} 0 \quad , & t \leqslant 0, \\ \cos\omega_0 t - 1, & 0 < t \leqslant \xi, \\ 0 \quad , & t > \xi. \end{cases} \tag{50}$$

Hence, η, which is the sum of η_1 and η_2, is given by

$$\eta = \frac{A_0}{a} \sum_{n=0}^{\infty} \frac{\omega_0^2 \tanh(k_n h) J_0(k_n r)}{k_n(p_n^2 - \omega_0^2) J_0(k_n a)} \begin{cases} 0 & , \quad t \leqslant 0, \\ \cos p_n t - \cos \omega_0 t & , \quad 0 < t \leqslant \xi, \\ \cos p_n t - \cos p_n (t-\xi), & t > \xi, \end{cases} \tag{51}$$

where the zero-order term is taken as $\lim_{k_n \to 0} . \eta_t$ and η_{tt} can be obtained as successive time differentiations of (51). η, η_t and η_{tt} are plotted for various values of t and for $a = 1{\cdot}35$ in., $\xi = 0{\cdot}01$ sec, $A_0 = 0{\cdot}01$ in., $h = 2{\cdot}5$ in., $g = 387$ in./sec^2, and $\tau = 4{\cdot}34$ in.^{3}/sec^2 in figure 13.

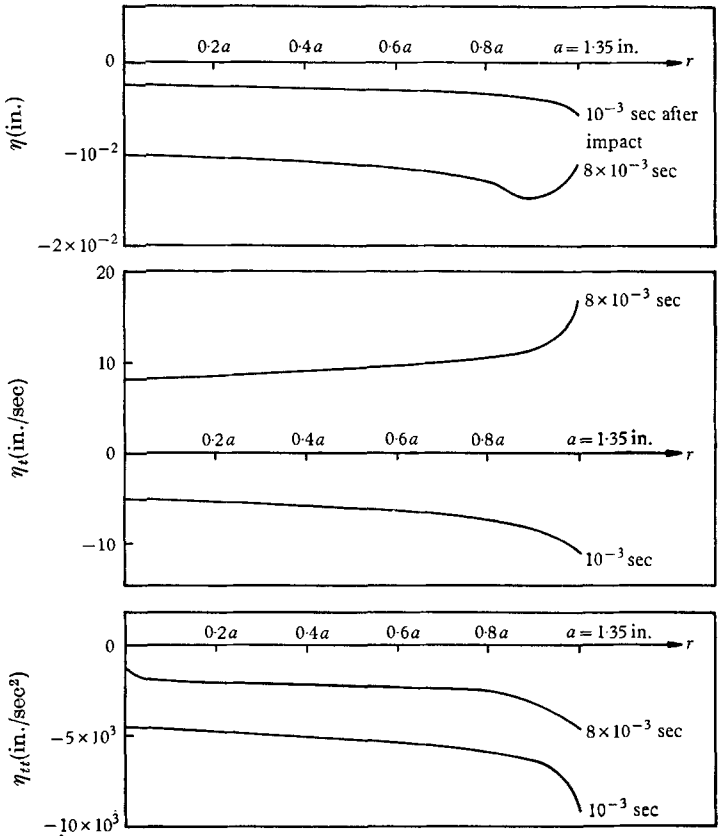

FIGURE 13. Free surface elevation, velocity, and acceleration at 10^{-3} and 8×10^{-3} sec after commencement of wall motion for the example carried out in the appendix.

REFERENCES

BENJAMIN, T. B. & URSELL, F. 1954 The stability of the plane free surface of a liquid in vertical periodic motion. *Proc. Roy. Soc.* A **205**, 505.

DODGE, F. D., KANA, D. D. & ABRAMSON, H. N. 1965 Liquid surface oscillations in longitudinally excited rigid cylindrical containers. *AIAA J.* **3**, 685.

JOHNSON, V. 1965 Cavitation. *Fourteenth American Towing Tank Conference.*

KNAPP, R. T. 1958 Cavitation and nuclei. *Trans. A.S.M.E.* p. 1315.

LEWIS, D. J. 1950 The instability of liquid surfaces when accelerated in a direction perpendicular to their planes. II. *Proc. Roy. Soc.* A **202**, 81.

RAYLEIGH, LORD 1879 On the instability of jets. *Proc. London Math. Soc.* **10**, 4.

TAYLOR, G. I. 1950 The instability of liquid surfaces when accelerated in a direction perpendicular to their planes. I. *Proc. Roy. Soc.* A **201**, 192.

TAYLOR, G. I. 1953 An experimental study of standing waves. *Proc. Roy. Soc.* A **218**, 44.

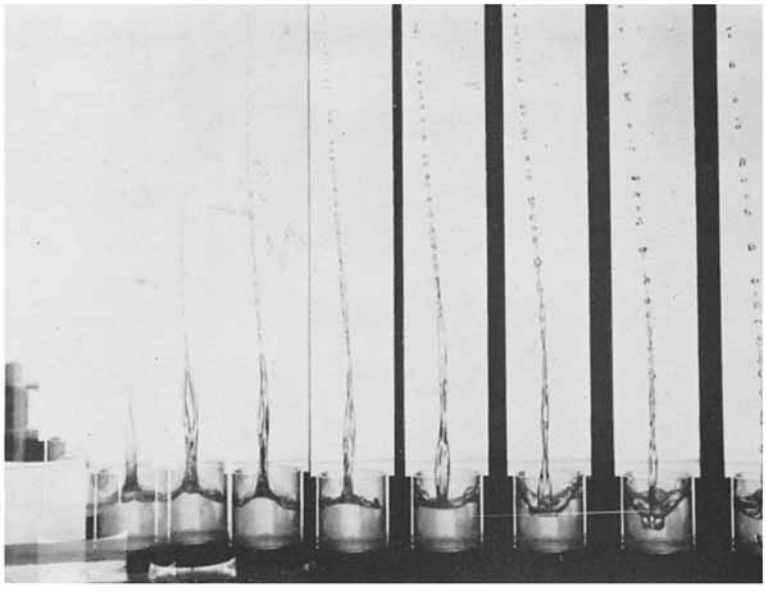

(*a*)

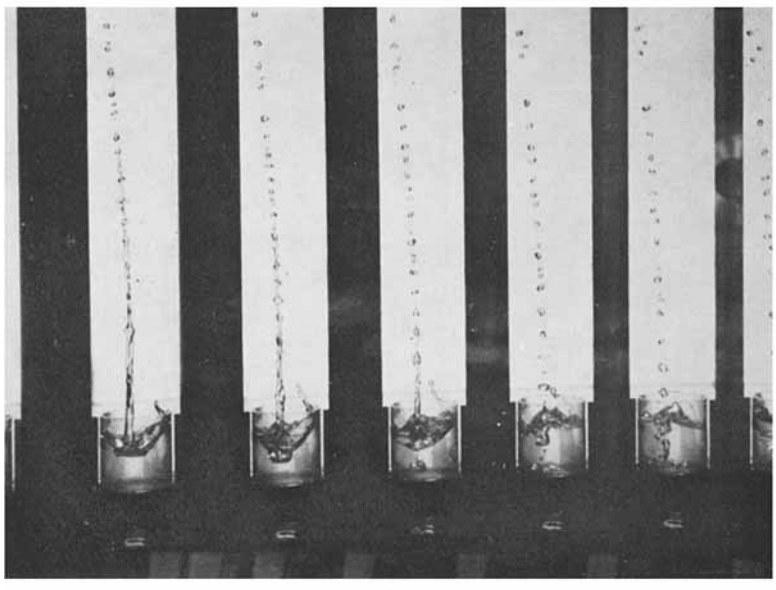

(*b*)

FIGURE 1. A sequence of photographs taken 0·033 sec apart of a vessel following vertical impact. Vessel contains ordinary tap water. (*a*) Beginning just before impact (note that the vessel bounced). (*b*) Beginning approximately 0·17 sec after impact.

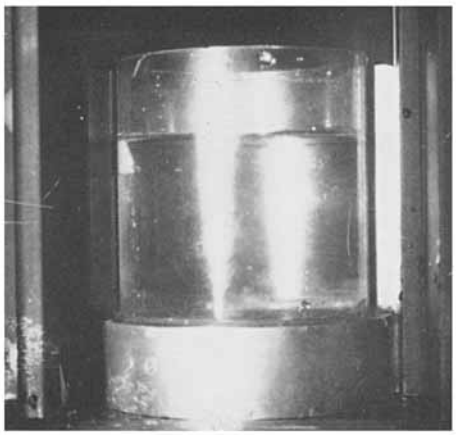

Tap water

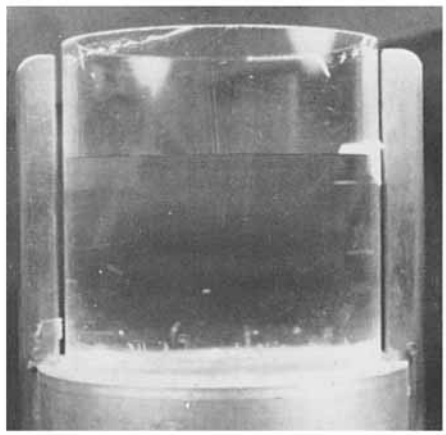

Deaerated tap water

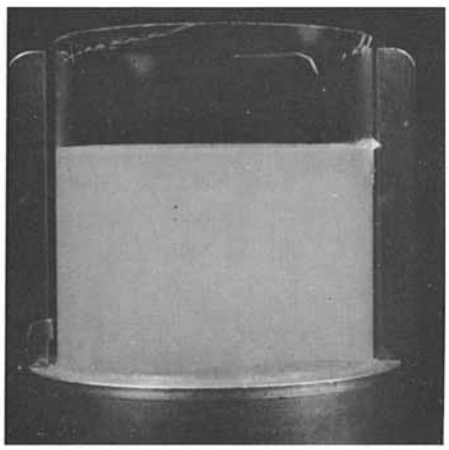

Soap solution

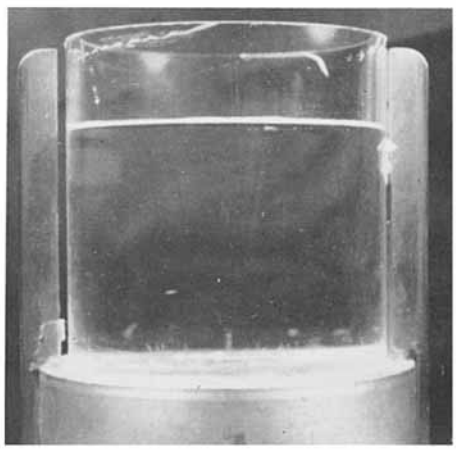

Glycerin

FIGURE 3. Photographs of the vessel, containing each of the four fluids used in the experiments at rest. Note the height of the meniscus in each case.

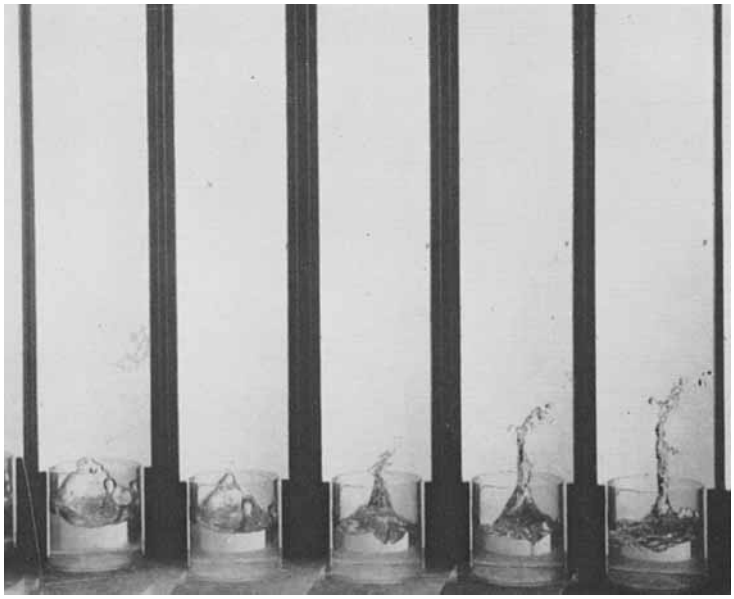

FIGURE 4. A sequence of photographs of the vessel containing deaerated water taken 0·033 sec apart following impact.

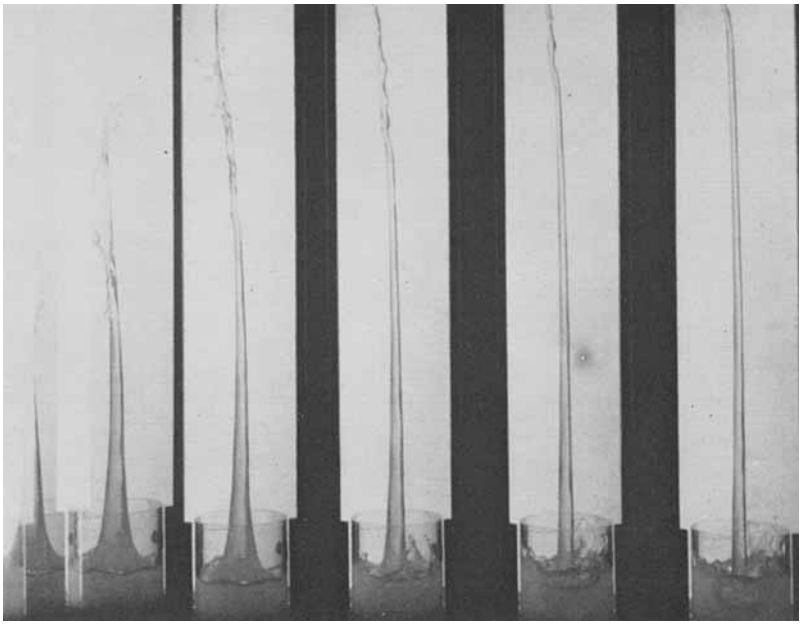

FIGURE 5. A sequence of photographs of the vessel containing soap solution taken 0·033 sec apart following impact.

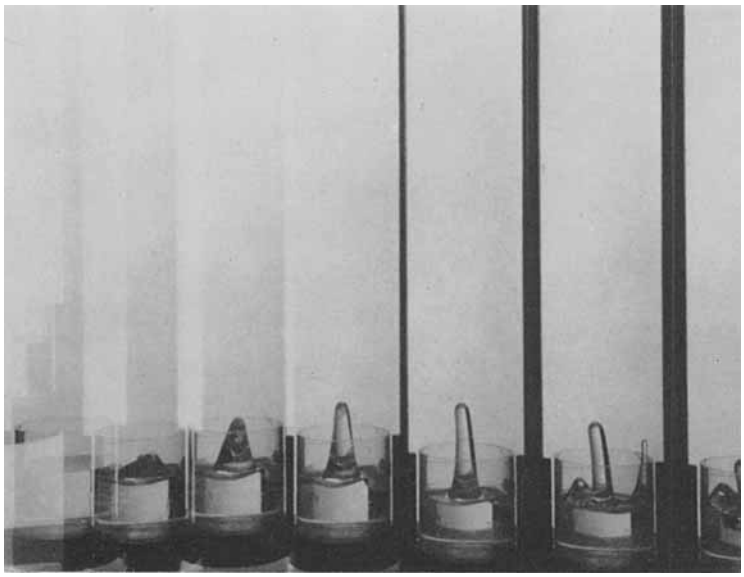

FIGURE 6. A sequence of photographs of the vessel containing glycerin taken 0·033 sec apart following impact.

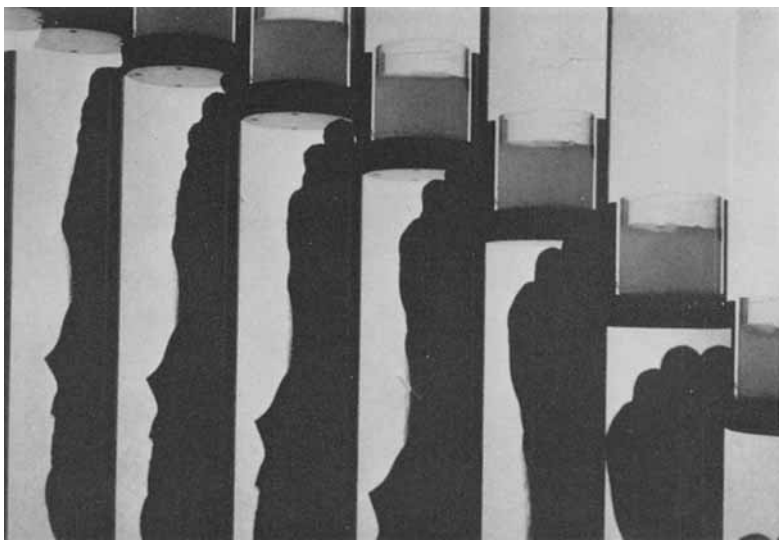

FIGURE 7. A sequence of photographs of the vessel containing soap solution taken 0·033 sec apart just as the vessel is released from rest. Note the motion of the free surface during free fall.

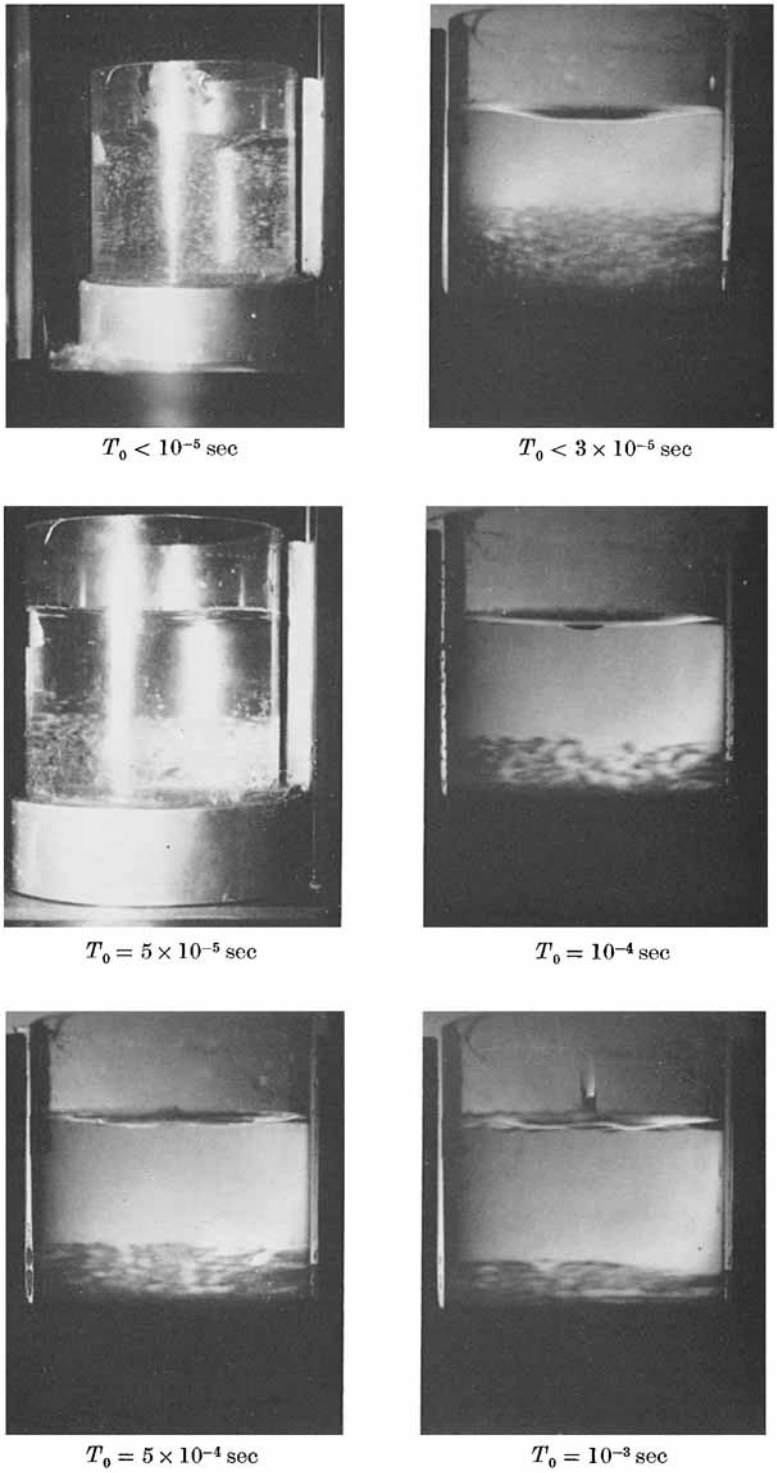

FIGURE 8. Photographs taken very shortly after vertical impact of a vessel containing ordinary tap water. Each photograph is of a different impact with a different time delay, T_0, between the time of impact and the time of taking the photograph.

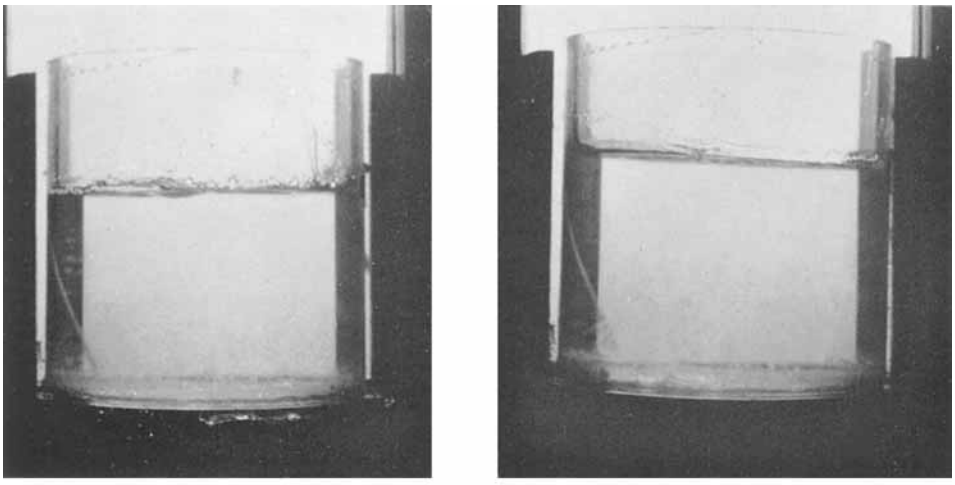

$T_0 < 10^{-5}$ sec $T_0 = 10^{-3}$ sec

FIGURE 9. Photographs of the vessel containing deaerated water at a time delay T_0 after impact.

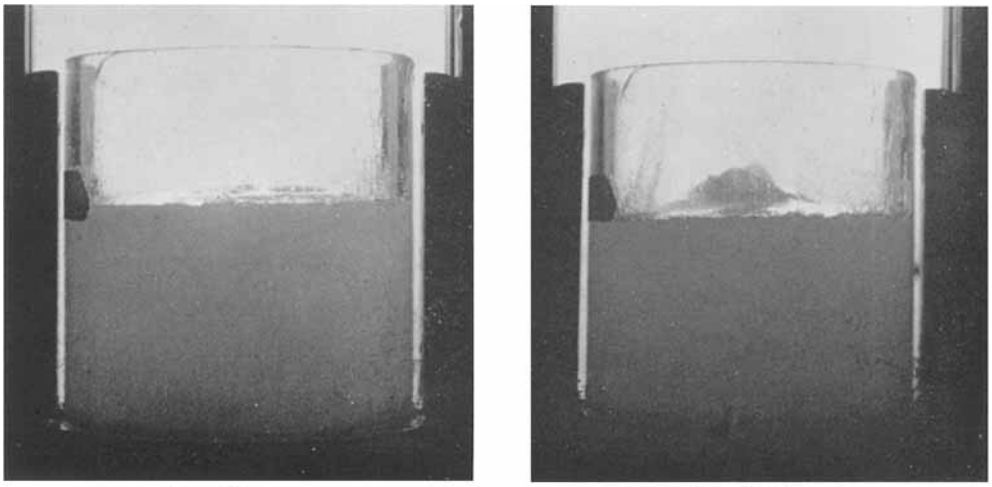

$T_0 < 10^{-5}$ sec $T_0 = 10^{-3}$ sec

FIGURE 10. Photographs of the vessel containing soap solution at a time delay T_0 after impact.